Carbohydrate Polymers 157 (2017) 105–113

Contents lists available at ScienceDirect

Carbohydrate Polymers

journal homepage: www.elsevier.com/locate/carbpol

Spray freeze-dried nanofibrillated cellulose aerogels with thermal superinsulating properties

Clara Jiménez-Saelices [a,b,c], Bastien Seantier [a,*], Bernard Cathala [b], Yves Grohens [a]

[a] IRDL, UBS, FRE CNRS 3744, F-56100 Lorient, France
[b] UR1268 Biopolymères Interactions Assemblages, INRA, F-44316 Nantes, France
[c] Agence de l'environnement et de la Maîtrise de l'Energie 20, avenue du Grésillé-BP 90406, 49004 Angers, France

ARTICLE INFO

Article history:
Received 28 June 2016
Received in revised form 8 September 2016
Accepted 22 September 2016
Available online 22 September 2016

Keywords:
Nanofibrillated cellulose (NFC)
Aerogel
Freeze-drying
Nano structure formation
Thermal superinsulation

ABSTRACT

Nanofibrillated cellulose (NFC) aerogels were prepared by spray freeze-drying (SFD). Their structural, mechanical and thermal insulation properties were compared to those of NFC aerogels prepared by conventional freeze-drying (CFD). The purpose of this investigation is to develop superinsulating bioaerogels by reducing their pore size. Severe reduction of the aerogel pore size and skeleton architecture were observed by SEM, aerogels prepared by SFD method show a fibril skeleton morphology, which defines a mesoporous structure. BET analyses confirm the appearance of a new organization structure with pores of nanometric sizes. As a consequence, the thermal insulation properties were significantly improved for SFD materials compared to CFD aerogel, reaching values of thermal conductivity as low as 0.018 W/(m K). Moreover, NFC aerogels have a thermal conductivity below that of air in ambient conditions, making them one of the best cellulose based thermal superinsulating material.

1. Introduction

Aerogels are highly porous materials with very low density and a large specific surface. They are prepared by replacing the solvent of a gel with gas with very moderate shrinkage of gel solid network. They form a class of materials showing potential for a wide range of applications (Hüsing & Schubert, 1998a) due to their unique optical (Platzer, Wittwer, & Mielke, 1986), mechanical (Gronauer, Kadur, & Fricke, 1986), and thermal properties (Fricke, 1988). Though the first aerogel was a silica aerogel made by (Kistler, 1931), intense research for new aerogels only began in the 1970's. Since then, inorganic aerogels have been extensively studied and used in several applications, including thermal insulating materials (Fricke, 1988), chemical adsorbents (Nguyen et al., 2014), drug carriers (Alnaief et al., 2012; Pierre & Pajonk, 2002), gas or liquid purifiers (Korhonen, Kettunen, Ras, & Ikkala, 2011) or in the aerospace industry (Jones, 2006).

In the context of a sustainable society, research is oriented towards the creation of aerogels from renewable resources. Thus, hybrid aerogels and bioaerogels are beginning to be studied (Alnaief, Alzaitoun, García-González, & Smirnova, 2011; Bendahou, Bendahou, Seantier, Grohens, & Kaddami, 2015; Borges et al., 2011; Cai et al., 2012; García-González, Alnaief, & Smirnova, 2011; Kistler, 1932; Koga et al., 2013). Bioaerogels are a new generation of aerogels prepared from biomass and most of them are prepared from polysaccharides. Cellulose is the most abundant polysaccharide on earth and it has been used for a large range of applications due to its renewability, biocompatibility and biodegradability (Huang, Yuan, & Chen, 2006). These properties are the reasons why, during the past decade, bioaerogels from cellulose have been developed (Cai, Kimura, Wada, Kuga,& Zhang, 2008; Gavillon & Budtova, 2008; Innerlohinger, Weber, & Kraft, 2006), cellulose derivatives (Fischer, Rigacci, Pirard, Berthon-Fabry, & Achard, 2006; Tan, Fung, Newman, & Vu, 2001) or nanofibrillated cellulose (NFC) (Pääkkö et al., 2008; Sehaqui, Zhou, & Berglund et al., 2011).

Some aerogels have a very low thermal conductivity at atmospheric pressure (Kistler, 1934). As a result, they form a new class of solids showing potentialities for insulating applications. Increasing research activity in bioaerogels has tried to improve their thermal properties in order to develop superinsulatingbioaerogels.

Thermal transfer in insulation materials can be divided into three contributions: conduction in a solid network, conduction in a gaseous phase and radiation through pores. The total thermal conductivity, λ, can be described by a parallel flux model (Eq. (1)) (Ebert, 2011) and calculated as the sum of each contribution (Fricke, 1986):

$$\lambda = \lambda_{solid} + \lambda_{gas} + \lambda_{rad} \quad (1)$$

* Corresponding author.
E-mail address: bastien.seantier@univ-ubs.fr (B. Seantier).

http://dx.doi.org/10.1016/j.carbpol.2016.09.068
0144-8617/

In aerogels, solid conduction is reduced compared to non-porous materials, because of the large quantity of pores which restricts the propagation of phonons in the aerogel skeleton (Fricke & Emmerling, 1992). The gas contribution is due to the elastic collision between gas molecules. To reduce it, a 3D mesoporous structure having specific size can be used. In porous materials, this specific size is characterized by the Knudsen number which is the ratio of the free mean path of gas molecules, l_g and the diameter of the pore, d (Eq. (2)) (Kaganer, 1969).

$$K_n = l_g/\mathrm{d} \quad (2)$$

Biobased aerogels are usually obtained from hydrogels since most biopolymers are soluble in water. Drying techniques such as freeze-drying, produce materials initially known as cryogels, now also termed aerogels (Pierre & Pajonk, 2002). During the freeze-drying technique, the gel is first frozen and then dried under low pressure by sublimation of the frozen liquid. The problem is that the gel network may be destroyed by nucleation and growth of solvent crystals (Tamon, Ishizaka, Yamamoto, & Suzuki, 2000). This effect tends to create structures with very large pores. Supercritical drying can avoid the collapse of aerogel structures during liquid removal by removing the liquid/vapor surface tension and thus achieving structures with nanoporosity (Kistler, 1931). Supercritical drying is, therefore, the most commonly used method to make aerogels (Baetens, Jelle, & Gustavsen, 2011). Only a few thermal superinsulating bioaerogels have been reported to date and they were made by supercritical drying. One was prepared from pectin by Rudaz et al. (2014), it has a pore size around 40 nm and a thermal conductivity of 0.016–0.020 W/(m K). Another example is a NFC bioaerogel with a thermal conductivity of 0.018 W/(m K) and pore sizes of 2–50 nm prepared by Kobayashi, Saito, & Isogai (2014). The size of the pores is the reason why there is no aerogel made by freeze-drying with superinsulatingproperties in the literature. The best values reported for aerogels prepared by freeze-drying are around 0.029–0.030 W/(m K) (Nguyen et al., 2014; Shi, Lu, Guo, Sun, & Cao, 2013). The major drawback of this technique is that resulting macroporous structures yield relatively high thermal conductivities because the contribution of gas conduction remains rather high.

In this study, we aim at overcoming this drawback by implementing spray freeze-drying technique (SFD) to reduce the aerogel pore size down to nanometric scale. SFD is an emerging technology utilized in many industries for the production of powders (Mujumdar, 2014). This process has two main steps: first, the solution is sprayed in a cryogenic solvent and the droplets are instantly frozen into micro granules. In the second step, frozen droplets are dried by sublimation. Originally, this technique was used to study the surface area of protein particles (Benson & Ellis, 1948) and afterwards it was used for the production of sub-micron powders (Werly & Baumann, 1964). Later, SFD has been used for a wide range of applications such as food elaboration (Malecki, Shinde, Morgan, & Farkas, 1970), pharmaceutical industry (Amorij et al., 2007; Cheow, Ng, Kho, & Hadinoto, 2011) or ceramic fabrication (Capadona, Shanmuganathan, Tyler, Rowan, & Weder, 2008; Shanmugam, 2015). More recently, it has also been used to prepare aerogel microspheres from NFC (Cai et al., 2014).

The advantage of this technique is that, thanks to the fast freezing, the gel structure is protected against deformation due to ice crystal growth. It is precisely this aspect that inspired us to adapt this method to the preparation of monolithic bioaerogels. Their structural, mechanical and thermal insulation properties were compared with those of bioaerogels made by CFD. The morphologies of these aerogels were examined using scanning electron microscopy (SEM) together with microstructural characteristics that were determined by nitrogen adsorption. Finally, mechanical and thermal insulation properties were determined. This work demonstrates that the preparation of bioaerogels with nanoporous structures by the SFD technique significantly improved thermal insulation properties.

2. Materials and methods

2.1. Materials

A 1 wt% aqueous suspension of NFC produced by TEMPO-mediated oxidation (Saito, Nishiyama, Putaux, Vignon, & Isogai, 2006) of spruce wood pulp was received from Swiss Federal Laboratories for Materials Science and Technology (EMPA, Dübendorf, Switzerland). The suspension was further characterized in order to confirm the supplier specifications. The 1.12 mmol/g carboxylate content was confirmed by conductimetric titration (SCAN-CM65:02, 2002). The dimensions were determined by AFM. The diameter and the length of the NFC were analyzed from 100 height pictures. The height of the NFC was considered to estimate the diameter in order to limit tip convolution effect. A 3.85 ± 0.98 nm NFC diameter and a minimum length of 450 nm were determined, which was in good agreement with the EMPA's specifications.

2.2. Aerogel preparation

Bioaerogels were prepared via concentration – drying route (Fig. 1). Concentrations of NFC dispersion were achieved by osmotic concentration using dextran solutions. NFC dispersion were placed in a dialyses membrane Espectra/Por® with a cutoff of 12–14 kDa and the dialyses membrane was immersed in a dextran solution at 10 wt%. Dextran is a complex branched glucan with a high molar mass, in this case 100 000 g/mol. During this process, the dextran solutions are changed every 30 h. Final concentrations of hydrogels varied from 1 wt% to 2.64 wt% (Fig. 1a). The drying process was compared between CFD and SFD. In both cases the process has two major steps: the freezing and the drying by sublimation of frozen water (Fig. 1b). The major difference between both processes is the freezing step. In the case of CFD, NFC hydrogels were poured into molds at room temperature and then placed in a deep-freeze at −80 °C for 24 h. In SFD, NFC hydrogels were sprayed inside molds that were cooled down to −80 °C. The hydrogels were atomized at 1.5 bar constant pressure through a 0.3 mm inner diameter steel nozzle. In both cases drying is carried out for 48 h using a Christ Alpha 1–2 LD Plus freeze-dryer. During freeze-drying, the condenser temperature was below −50 °C and the vacuum was below 0.1 mbar.

2.3. Characterization

2.3.1. Bulk density

Bulk density ρ_{bulk} of the aerogels was calculated by dividing their weight by their volume, which was measured by a digital caliper. Weight of aerogels was measured with an analytical balance Mettler Toledo XS. In addition to this, porosity was calculated from Eq. (3) where the ratio $\rho_{bulk}/\rho_{skeletal}$ is the relative density. Skeletal density $\rho_{skeletal}$ is the density of cellulose, 1.6 g/cm^3 (Ganster & Fink, 1999).

$$\varepsilon(\%) = (1-(\rho_{bulk}/\rho_{\mathrm{skeletal}}))\mathrm{x}100 \quad (3)$$

2.3.2. Scanning electron microscopy (SEM)

A JEOL JSM 6460LV scanning electron microscope operating at 20 kV was used to capture structural images of the bioaerogels. Thin layers of gold were deposited by sputtering with scan-coat onto the surface of the cross sections. Aerogel samples were prepared for SEM observation by cryo-fracture in liquid nitrogen.

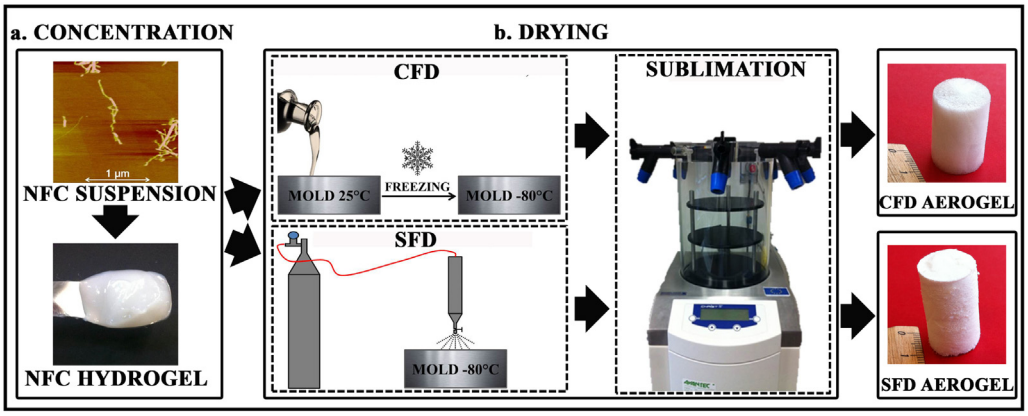

Fig. 1. Bioaerogels preparation. a) from the NFC suspension, hydrogels were obtained by osmotic concentration. b) aerogels were produced by CFD and SFD.

2.3.3. BET analysis

Nitrogen adsorption-desorption isotherms were obtained using a Micromeritics TriStar 3000 apparatus. The bioaerogel samples were placed in the measuring cell to remove all water molecules adsorbed. The material was degassed by heating at 100 °C for 24 h. We chose relatively mild degassing conditions in order not to degrade the sample and to be sure that all the water molecules were removed. Subsequently, the measuring cell is placed in an insulated tank filled with liquid nitrogen. This keeps the sample at −196 °C throughout the measurement, a temperature at which gaseous nitrogen adsorption is possible on a solid surface. A nitrogen adsorption-desorption isotherm represents the evolution of the volume of nitrogen adsorbed per gram of sample extrapolated to standard conditions of temperature and pressure (cm^3/g STP) depending on the relative pressure of nitrogen (P/P_0). Using the BET theory (Brunauer, Emmett, & Teller, 1938), it is possible to evaluate the specific surface area. The average pore size of the NFC aerogels was estimated from the nitrogen desorption isotherm (Micromeritics TriStar 3000) according to the BJH method (Barret, Joyner, & Halenda, 1951).

2.3.4. Mechanical characterization

Uniaxial compression experiments were performed in a Instron 5566A using a load cell of 100 N for precise measurements of Young modulus and 1 kn for complete stress-strain curve of high density aerogels. The aerogels were placed between two parallel plates and planarity and parallelism were verified with a micrometric sensor. The tests were performed at atmospheric pressure in a temperature and humidity controlled room (21–22 °C and 50% relative humidity). The displacement rate was 1 mm/min and tests were done until exceed 70% of sample deformation. The samples were cylinders with the ratio length/diameter = 3/2. At least three samples per formulation were tested.

2.3.5. Thermal conductivity measurements

Thermal conductivity, λ, of the sample is measured in the steady state using the hot strip technique. The hot strip technique (Fig. 2) consists on a homemade device constituted by an isothermal aluminum case (Fig. 2[4]) with two cavities, one containing polyurethane foam (Fig. A1[2]) while the other contains the sample to be characterized (Fig. 2[1]). These two cavities are symmetrically positioned with respect to a strip (Fig. 2[3]) that is electrically isolated from the case (Fig. 2[5]). Two electrodes (Fig. 2[6]) provide the electrical power supply to the strip and two thermocouples (Fig. 2[7]) measure the temperature of both the strip and the case while the temperature of the case is kept constant by a cooling circuit.

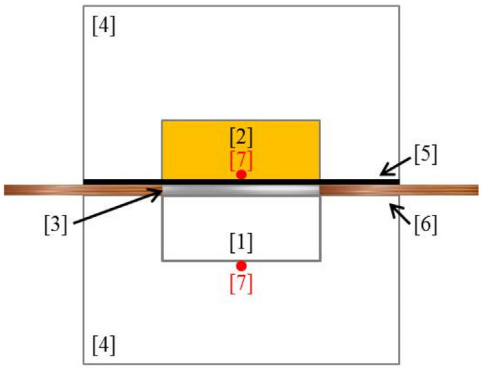

Fig. 2. Hot strip device. [1] Sample. [2] Polyurethane foam. [3] Strip NiCr. [4] Isothermal aluminum case. [5] Electrical insulator. [6] Electrodes (copper). [7] Thermocouples.

This device, adapted from the hot filament technique, has been previously developed for thermal characterization of aerogels (Bendahou et al., 2015; Gustafsson, Karawacki, & Khan, 1979). The tests were performed at atmospheric pressure in a temperature and humidity controlled room (21–22 °C and 50% relative humidity). At least five samples per formulation were tested.

3. Results and discussion

3.1. Aerogel density, morphology and microstructural characteristics

3.1.1. Texture and density of the bioaerogels

Bioaerogels were prepared from NFC suspensions by CFD and SFD methods. Monolithic and homogeneous aerogels were successfully obtained, as shown in Fig. 1 (see also Fig. S4 in Supporting information).

The bulk density of bioaerogels as a function of the NFC concentration is illustrated in Fig. 3. The theoretical density (red solid line in Fig. 3) was calculated assuming there was no volume shrinkage between the gel (precursor of the aerogel) and the aerogel (dried sample). The bioaerogels prepared from NFC within the present study have densities varying between 0.012 and 0.033 g/cm^3 with the NFC concentrations varying between 1 and 2.64 wt% (Fig. 3). The bulk density of the aerogels increases in an almost linear manner with the NFC concentration for both drying techniques, which has already been demonstrated and reported (Aulin, Netrval, Wågberg, & Lindström, 2010; Hoepfner, Ratke, & Milow, 2008; Kobayashi et al., 2014; Sescousse, Gavillon, & Budtova, 2011). The porosity

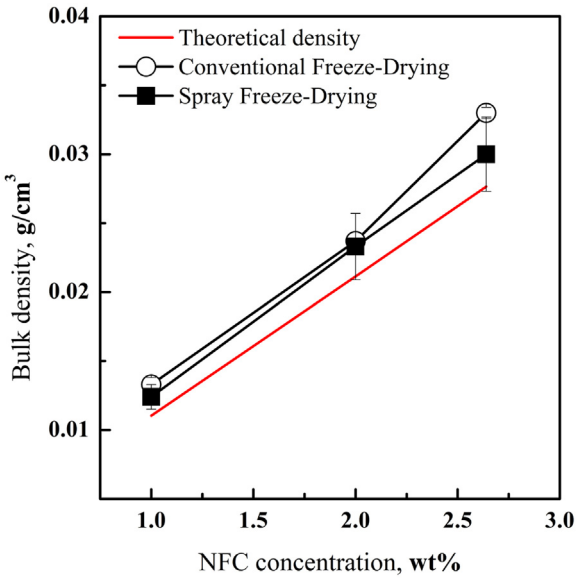

Fig. 3. Bulk densities of bioaerogels made by CFD (open circles) and by SFD (dark squares). Black solid lines show the dependence of bulk density with concentration. The red line is the theoretical density, which is calculated assuming there is no volume shrinkage. (For interpretation of the references to colour in this figure legend, the reader is referred to the web version of this article.)

varied from 99% for the aerogels from 1 wt% NFC suspension to 98% for aerogels obtained from 2.64 wt% suspension.

The drying technique does not have a great influence on the bioaerogels density or porosity and both drying techniques achieve very low density and high porosity bioaerogels with no significant shrinkage. Aerogels based on polysaccharide derivatives have fairly high densities (0.25–0.85 g/cm^3) and low porosities (85–41%) (Fischer et al., 2006). They typically consist of densely crosslinked chains which can cause a large shrinkage (20–60%). Instead, nanofibers are flexible and they are entangled with each other, creating networks even at very low concentrations. This means that a lower cellulose concentration can be used to fabricate monolithic aerogels (Pääkkö et al., 2008). These factors can explain why the present bioaerogels have a lower density and higher porosity compared to bioaerogels already reported in the literature (Fischer et al., 2006; Tan et al., 2001).

3.1.2. Morphology of the bioaerogels

The morphologies of bioaerogels are highly influenced by the drying technique used, as illustrated by the SEM images (Fig. 4). A 2D-sheet-like morphology is observed for bioaerogels prepared by CFD (Fig. 4a–c). This morphology is commonly observed in the literature for bioaerogels made by CFD when the NFC concentration exceeds 0.5 wt% (Aulin et al., 2010; Bendahou et al., 2015; Chen, Wang et al., 2014; Silva, Habibi, Colodette, Elder, & Lucia, 2012). In contrast, when bioaerogels are made by SFD, a three dimensional fibrillar skeleton morphology is obtained (Fig. 4d–f). A similar morphology was reported for bioaerogels made by supercritical drying of cellulose (Gavillon & Budtova, 2008) or NFC (Kobayashi et al., 2014).

The freeze-drying process consists of two steps: freezing and drying. However the final architecture of aerogel significantly depends on the freezing stage. In fact, the distribution of pore size, the shape and the connectivity of the porous network is the result of the shape of ice crystals that are formed during freezing (Kiani & Sun, 2011; Liapis, Pim, & Bruttini, 1996).

In CFD, NFC dispersion is frozen inside molds. During the nucleation stage, the first cores of ice are formed and the fibers are separated from frozen water. Then, large ice crystals grow in the direction of the temperature gradient (Deville, 2008). During this growth, the fibers are confined to the interstitial regions, which causes an increase in the concentration between the ice crystals. Therefore, the large formed crystals restrict the space for the fibers. NFC are organized along the growth direction of the ice crystals due to the effect of compression between several ice crystals (Chen, Schueneman, Pipes, Youngblood,, & Moon, 2014). Concentrated and confined, the NFC undergo a lateral agglomeration (Hult, Larsson, & Iversen, 2001) and change into a 2D-sheet-like morphology. After the freezing is complete, the frozen water is removed by sublimation. Hydrogen bonds and van der Waals forces hold the nanofibers together after the removal of water (Hunter, 2001) and the structure is therefore directly related to the size and distribution of the ice crystals in the frozen system (Thybo, Hovgaard, Andersen, & Lindeløv, 2008).

For SFD, NFC suspensions are sprayed onto a surface at −80 °C. The small droplets, with diameters ranging around few tens of micrometers (Thybo et al., 2008), form thin layers of NFC dispersions onto the spraying surface. The thickness of sample droplets layer plays an important role on the kinetic of ice formation, with higher cooling rates for thinner sample layers (Aulin et al., 2010). Rapid cooling is accompanied by the formation of amorphous ice and a very limited crystal growth step. As a consequence, the NFC do not have time to agglomerate and a 3D-fibril skeleton structure with smaller pore size is obtained for the aerogel (Jennings, 1999). During the sublimation of the separated ice crystals, strong hydrogen bonds formed between the hydroxyl groups of adjacent NFC surfaces hold the structure to obtain a 3D-fibril skeleton morphology at the end of the process (Chen, Schueneman et al., 2014).

3.1.3. Structure of aerogels performed by adsorption/desorption of nitrogen

Nitrogen adsorption was used to determine the specific surface area and porosity characteristics of the NFC aerogels. There is no adsorption in the case of NFC aerogels prepared by CFD and the estimated specific surface area is around 1 m^2/g, which is characteristic of non-porous or macroporous solids. These results correspond to the SEM images (Fig. 4a–c) showing a 2D-sheet-like morphology with large pores resulting from large water crystals. For bioaerogels prepared by SFD, all the sorption isotherms obtained were of type IV (Fig. 5) according to IUPAC classification (Rouquerol et al., 1994). The isotherms show a gradual increase of adsorbed nitrogen quantity with pressure and a hysteresis loop of type A during desorption. This is typical for mesoporous adsorbents with a strong adsorbate–adsorbent interaction (see Fig. 5 for a typical isotherm). The specific surface area S_{BET} is an important structural characteristic of aerogels; it was determined from the adsorption isotherms using BET analysis (Brunauer et al., 1938). S_{BET} of the SFD aerogels are almost constant within a narrow range of 80–100 m^2/g.

All bioaerogels have a significantly lower specific surface area compared to silica aerogels (800–1000 m^2/g) (Koebel, Rigacci, & Achard, 2012). Nevertheless, higher values were reported in literature for cellulose based bioaerogels obtained by supercritical drying than those we measured for SFD bioaerogels. Specific surface areas of cellulose aerogels or cellulose derivatives aerogels can be about twice the values we obtained (100–250 m^2/g) (Fischer et al., 2006; Gavillon & Budtova, 2008; Innerlohinger et al., 2006; Tan et al., 2001) and are in some cases significantly higher (500 m^2/g) (Cai et al., 2008). Nevertheless, in all these cases, the aerogels were prepared by supercritical drying. In freeze-drying, the pore volume of the gel changes during freezing, particularly in the case of water. The change of water density results in an expansion of around 10% after freezing which is not tolerated by the structure and may cause damage to the gel network (Reichenauer, 2000). This results in aerogels having larger pores inducing low specific surface area, such as NFC aerogels made by freeze-drying with S_{BET}

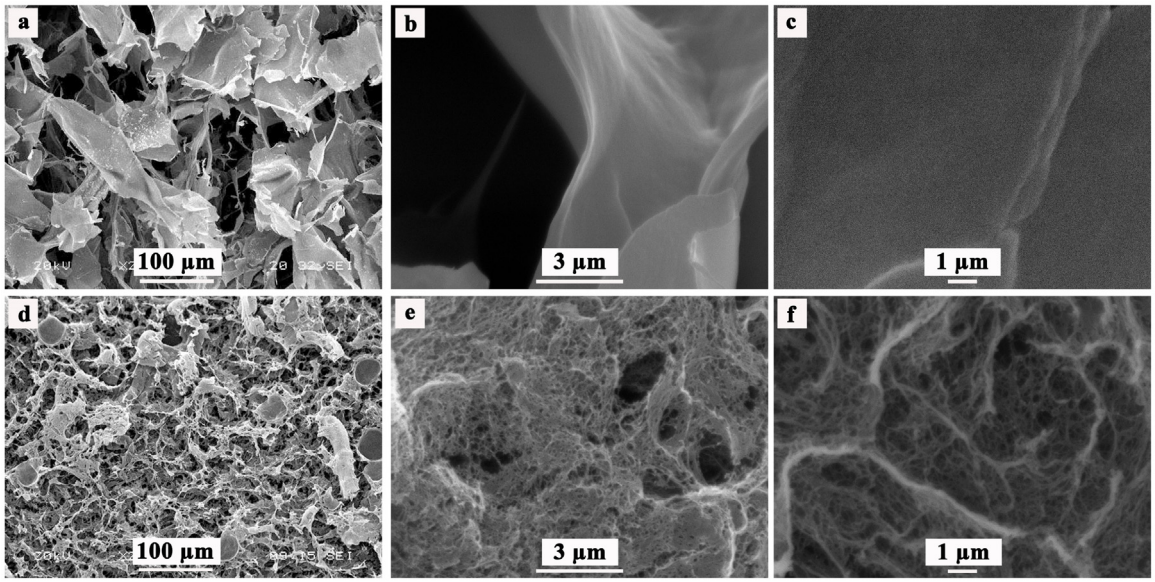

Fig. 4. SEM images of bioaerogels prepared from 2 wt% NFC solution by conventional freeze-drying (a–c) and spray freeze-drying (d–f).

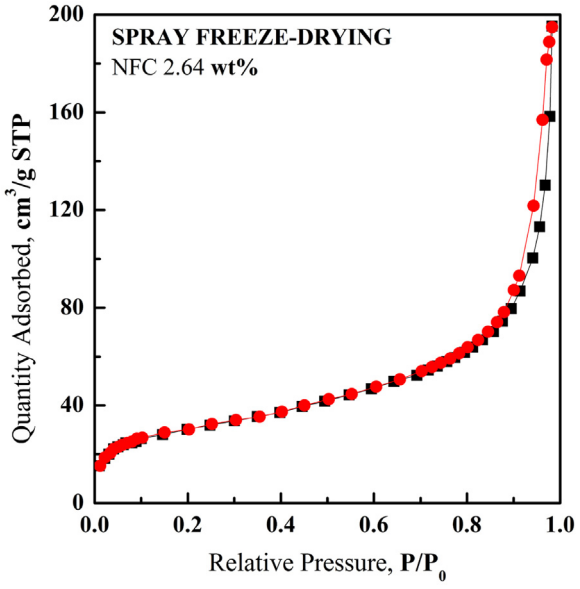

Fig. 5. Nitrogen adsorption-desorption isotherm obtained for bioaerogels prepared by SFD from NFC 2.64 wt% suspension. The absorbed nitrogen quantity is represented as a function of the relative nitrogen pressure.

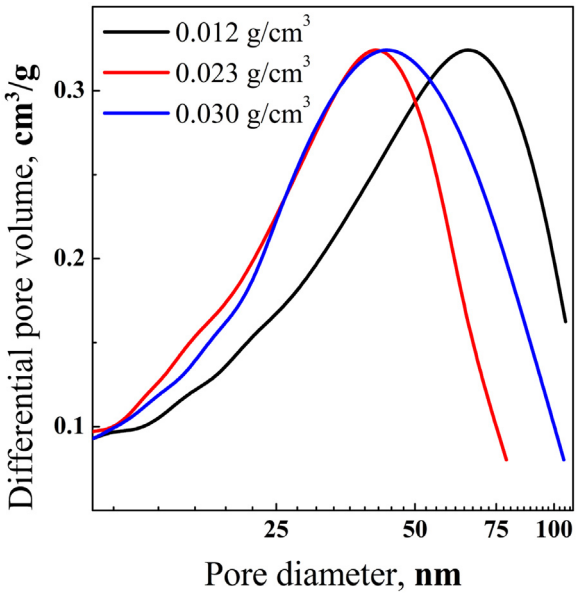

Fig. 6. Pore size distributions of SFD aerogels estimated from their nitrogen desorption isotherms followed by the BJH model.

lower than 40 m^2/g (Aulin et al., 2010; Jennings, 1999; Sehaqui, Salajková, Zhou, & Berglund, 2010). One way to avoid this problem is to increase the cooling rate. One example is the first NFC aerogel which was obtained by rapid freezing in liquid propane and that got a S_{BET} value around 70 m^2/g (Pääkkö et al., 2008). The present results have a high specific surface area (80–100 m^2/g) in comparison to those obtained for bioaerogels made by freeze-drying. We can thus suppose that the cooling rate is faster in the SFD process even if the freezing temperature is lower (ca −80 °C for SFD method vs ca −180 °C for liquid propane). Consequently SFD allows a higher nanostructuration in contrast with CFD as demonstrated by the results of this study. To confirm our hypothesis we measured the pore size distribution using the BJH approach (Barret et al., 1951). Nitrogen adsorption-desorption method measures a very limited fraction of pore volume and this fraction is smaller as the aerogel density decreases. However the BJH model has been widely used to estimate pore size distribution for all kinds of aerogels (Kobayashi et al., 2014; Pääkkö et al., 2008; Sehaqui, Zhou, Ikkala, & Berglund, 2011; Silva et al., 2012). In this study we used this model to assess the presence of mesoporosity in the SFD aerogel. Since the CFD aerogels are macroporous, pore size cannot be determined by the BJH model. For bioaerogels prepared by SFD, the pore size distribution estimated from the isotherms range from 10 to 100 nm. While the most probable diameter is around 70 nm for a concentration of NFC 1 wt%, it is only around 40 nm for a concentration of NFC 2 wt% or 2.64 wt% (Fig. 6).

The mean pore size, L_p is estimated according to Eq. (4):

$$L_p = 4 \cdot V_{exp}/S_{BET} \quad (4)$$

Where V_{exp} is the measured cumulated pore volume per gram of matter. The L_p of SFD bioaerogels is around 10 nm, which is similar to the diameters found in literature for bioaerogels prepared by

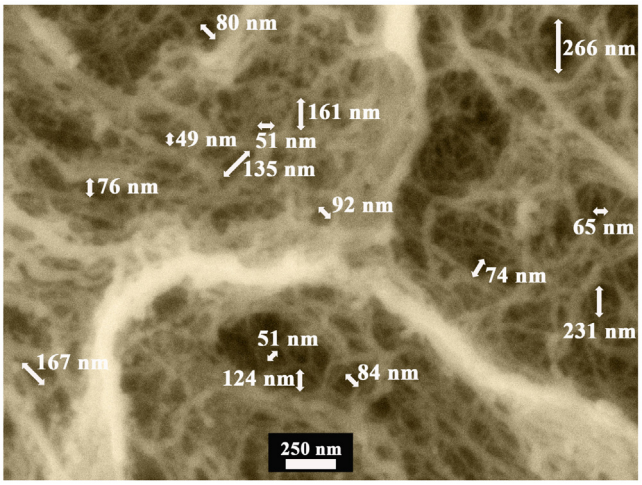

Fig. 7. SEM image of SFD aerogel prepared from 2 wt% NFC solution with few examples of pore size.

supercritical drying (Fischer et al., 2006; Kobayashi et al., 2014; Rudaz et al., 2014; Tan et al., 2001). SEM images for SFD aerogels show that pores can be larger than these results and reach diameters even up to a few micrometers (Fig. 7). The discrepancies between the pore sizes measured by the BJH approach or directly on the SEM images are entirely reasonable. First, because each technique works in a different scale, macroporous are visible in SEM images while they are not measurable using the BJH approach. Finally, because only a tiny fraction of the total pore volume is analyzed with nitrogen adsorption-desorption measurements. However, despite finding large pores, the SEM images show a large number of pores in the same order of magnitude as the BJH approach results and in any case within the mesoporous domain (Fig. 7).

Altogether, these results indicate that morphology, specific surface area and pore size of NFC aerogels can be highly influenced by the drying technique. The SFD enables the creation of bioaerogels with a very low density, a 3D-fibril skeleton morphology, and an ultra-porous system with mesoporous domains and specific surface area around 80–100 m^2/g.

3.2. Mechanical properties

The mechanical properties of aerogels were studied by uniaxial compression. No changes in the cross section area and no buckling were observed during the experiments. That means the Poisson ratio is close to zero. The compressive modulus, yield stress σ_{yield} (beginning of plastic region), the yield strain ε_{yield} and the energy absorbed by the sample from the beginning of deformation to 40% strain, $W_{40\%}$ were determined.

Representative stress-strain curves of CFD and SFD aerogels are presented together in Fig. 8a. For both kinds of aerogels, the compressive modulus, the yield stress and the absorbed energy increase with the increase of bulk density (see details in Table S1 in Supporting information). The increase of bulk density leads to an increase of the pore wall thickness causing a higher resistance of the structure to cell wall bending and collapse. This behavior has already been observed for foam structures and aerogels (Kobayashi et al., 2014; Rudaz et al., 2014; Sehaqui et al., 2010; Sehaqui, Zhou, Berglund et al., 2011). However between CFD and SFD aerogels the mechanical behavior differs.

CFD aerogels show typical compressive stress-strain curves where three regions can be distinguished. A linear elastic region at low strains (<3%) from which compressive modulus can be determined, a long plastic deformation region characterized by a stress plateau and finally a densification region (Gibson & Ashby, 1999). However for SFD aerogels, the stress-strain curves show a strain hardening behavior already at low strain. The curve increases progressively until densification region and no yield stress can be detected. These kinds of curves, without a defined plastic region, have been reported for silica aerogels (Wong, Kaymak, Brunner, & Koebel, 2014), organic aerogels (Pekala, Alviso, & LeMay, 1990) or NFC aerogels (Sehaqui, Zhou, Berglund et al., 2011). As in literature, the compressive modulus was determined from the slope of the linear region of the curve. It is an apparent modulus because SFD aerogel is truly elastic only at strains below 3%.

CFD and SFD aerogels show distinct mechanical behaviors that can be explained by the aerogel microstructures. In CFD aerogels, the pore walls exhibit a 2D-sheet-like morphology. It results in a relatively high resistance to compression. For the same density, the 3D-fibril skeleton morphology of SFD aerogel induces a smaller pore wall thickness causing lower stress values for the same deformation. That is why the compression modules of SFD aerogels are lower than those of CFD aerogels (Fig. 8b). Furthermore, the pore walls touch each other progressively in a gradual hardening process, which makes the stress increasing linearly with strain.

Compressive moduli of aerogels are plotted as a function of bulk density in Fig. 8b. The CFD aerogels prepared in the present study show significantly improved compressive moduli compared to the literature. Not only far exceeding the values achieved for silica aerogels (Alaoui, Woignier, Scherer, & Phalippou, 2008) or NFC aerogels (Kobayashi et al., 2014; Sehaqui et al., 2010), the prepared aerogels reach moduli in the same order of magnitude than reported bioaerogels even if they have lower densities. For example, compressive moduli of 5.7 MPa are reached for CFD aerogels with a density of 0.033 g/cm^3. It is a density three times lower than the density of cellulose or pectin aerogels that have a similar compressive modulus (Rudaz et al., 2014; Sescousse et al., 2011; Svagan, Samir, & Berglund, 2008). In the case of SFD aerogels, the compression modulus reaches lower values, but they are still higher compared to silica aerogels (Alaoui et al., 2008; Wong et al., 2014). In addition, they are comparable to those found for other bioaerogels made also from NFC (Kobayashi et al., 2014; Sehaqui et al., 2010; Sehaqui, Zhou, Berglund et al., 2011), considering the low density of the aerogels presented in this work.

Looking at the shape of the stress-strain curves and how they change with the increase of density, it is expectable that a slight increase of density leads to a remarkable improvement of compressive modulus.

3.3. Thermal insulation properties

The total thermal conductivity of NFC aerogels was measured with the hot strip technique (see material and methods and Supported Information Fig. S1) and the results are given as a function of bulk density and are presented in Fig. 9.

Bioaerogels made by CFD have thermal conductivity varying between 0.024 and 0.028 W/(m K). With samples having the same range of densities, the aerogels prepared by SFD reach thermal conductivity values of 0.018–0.021 W/(m K). With the developed materials, both the contributions of the solid conduction (λ_{solid}) and the gas conduction (λ_{gas}) can be significantly reduced. By lowering the bulk density of the aerogel, the solid conduction contribution is reduced and by decreasing the pore size to less than the mean free path of air molecules (ca. 70 nm), it is the gas conductivity contribution that is lowered. The improvement of the thermal insulation properties of bioaerogels made by SFD compared to bioaerogels made by CFD is due to the contrast in their morphologies and microstructures. The macroporous structure of CFD aerogels allows the free circulation of air molecules and the conduction of heat

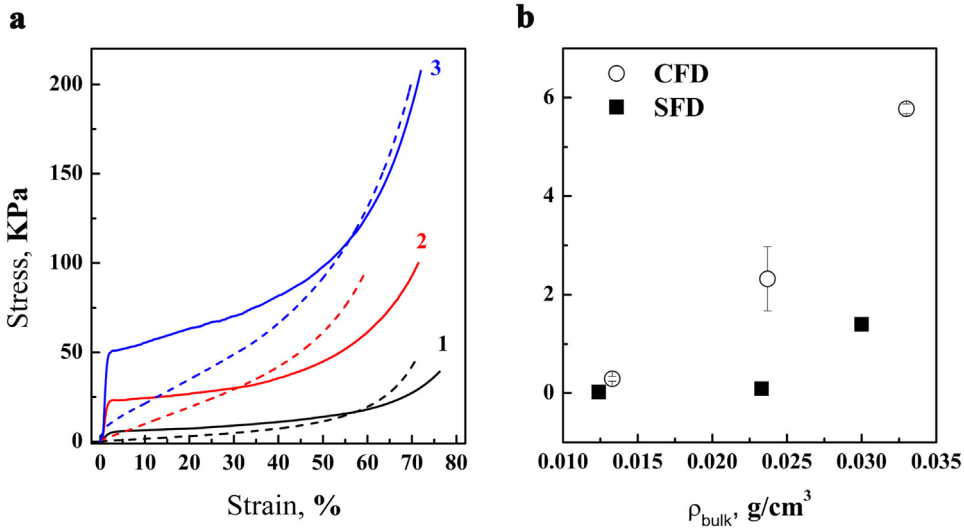

Fig. 8. (a) Example of stress-strain uniaxial compression curves for bioaerogels prepared from 1 (1), 2 (2) and 2.64 wt% (3) by CFD (solid lines) and SFD (dashed lines). (b) Compressive modulus as a function of bulk density for CFD and SFD aerogels.

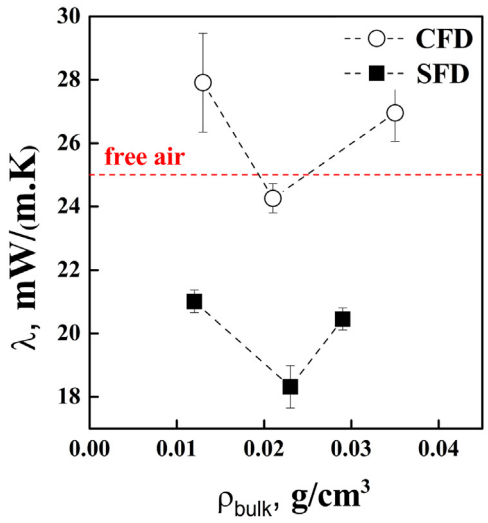

Fig. 9. Thermal conductivity of bioaerogels as a function of bulk density. Air thermal conductivity is represented by a dashed red line at 0.025 W/(m K). Dotted lines are guides for eyes. (For interpretation of the references to colour in this figure legend, the reader is referred to the web version of this article.)

by the chock between air molecules. However, the SFD aerogels ultra-porous structure with mesoporous domains favors the Knudsen effect. Indeed, the air molecules are confined inside pores smaller than their mean free path. As a result, the contribution of gas conduction decreases and thus the total thermal conductivity decreases too. The lowest thermal conductivity obtained for SFD bioaerogels is 0.018 W/(m K). This value is comparable to the lowest values reported in literature for bioaerogels made by supercritical drying, 0.016–0.018 W/(m K) (Kobayashi et al., 2014; Rudaz et al., 2014) and is lower than those of bioaerogels made by conventional freeze-drying, 0.029–0.032 W/(m K) (Nguyen et al., 2014; Shi et al., 2013).

In this study, low density and mesoporous bioaerogels were obtained. Their thermal insulation properties are better than those of commercially available insulators, such as polyurethane foam, carbonized cork, and mineral wools (0.03–0.05 W/(m K)) (Hüsing & Schubert, 1998b; Pierre & Pajonk, 2002). Therefore, SFD aerogels can be used as a novel high-performance thermal superinsulator.

4. Conclusions

In this article, bioaerogels were prepared from NFC suspensions by osmotic concentration followed by drying step done by CFD and SFD methods. Monolithic and homogeneous aerogels were successfully obtained. All bioaerogels have a very low density (0.012–0.033 g/cm^3) and a high porosity (98–99%). SEM characterization highlighted microstructure differences between both aerogels. When bioaerogels prepared by CFD exhibit a 2D-sheet-like morphology with macropores, bioaerogels made by SFD yield a 3D-fibril nanostructured skeleton morphology with pore size going from few tens of nanometers to few microns. Specific surface area of SFD aerogels was determined using nitrogen adsorption-desorption and the BET method. A value around 100 m^2/g was obtained. The average pore size of the SFD aerogels was estimated from the nitrogen desorption isotherm according to the BJH method. Results confirm the presence of mesoporous domains as it was found in SEM images. The mechanical properties of bioaerogels were measured by uniaxial compression. CFD aerogel structure offers superior resistance to compression than SFD structure allowing achieving higher compressive modulus. The most important result obtained in this study is that SFD aerogels have very low thermal conductivity. The best value obtained was 0.018 W/(m K). These are the first bioaerogels, prepared by another technique than supercritical drying, having thermal superinsulating properties. Therefore, the present study provides a new and effective method to prepare NFC aerogels with thermal superinsulating properties.

Acknowledgments

This work was supported by the French Environment and Energy Management Agency (ADEME) and Bretagne region. The authors thank Anthony Magueresse (IRDL, UBS, Rue de Saint Maudé, Lorient, France) for the SEM images.

Appendix A. Supplementary data

Supplementary data associated with this article can be found, in the online version, at http://dx.doi.org/10.1016/j.carbpol.2016.09.068.

References

Alaoui, A. H., Woignier, T., Scherer, G. W., & Phalippou, J. (2008). Comparison between flexural and uniaxial compression tests to measure the elastic modulus of silica aerogel. *Journal of Non-Crystalline Solids*, *354*(40–41), 4556–4561.

Alnaief, M., Alzaitoun, M. A., García-González, C. A., & Smirnova, I. (2011). Preparation of biodegradable nanoporous microspherical aerogel based on alginate. *Carbohydrate Polymers*, *84*(3), 1011–1018.

Alnaief, M., Antonyuk, S., Hentzschel, C. M., Leopold, C. S., Heinrich, S., & Smirnova, I. (2012). A novel process for coating of silica aerogel microspheres for controlled drug release applications. *Microporous and Mesoporous Materials*, *160*, 167–173.

Amorij, J. P., Saluja, V., Petersen, A. H., Hinrichs, W. L. J., Huckriede, A., & Frijlink, H. W. (2007). Pulmonary delivery of an inulin-stabilized influenza subunit vaccine prepared by spray-freeze drying induces systemic, mucosal humoral as well as cell-mediated immune responses in BALB/c mice. *Vaccine*, *25*(52), 8707–8717.

Aulin, C., Netrval, J., Wågberg, L., & Lindström, T. (2010). Aerogels from nanofibrillated cellulose with tunable oleophobicity. *Soft Matter*, *6*(14), 3298–3305.

Baetens, R., Jelle, B. P., & Gustavsen, A. (2011). Aerogel insulation for building applications: A state-of-the-art review. *Energy and Buildings*, *43*(4), 761–769.

Barret, E. P., Joyner, L. G., & Halenda, P. P. (1951). The determination of pore volume and area distributions in porous substances. Computations from nitrogen isotherms. *Journal of the American Chemical Society*, *73*(1), 373–380.

Bendahou, D., Bendahou, A., Seantier, B., Grohens, Y., & Kaddami, H. (2015). Nano-fibrillated cellulose-zeolites based new hybrid composites aerogels with super thermal insulating properties. *Industrial Crops and Products*, *65*, 374–382.

Benson, S. W., & Ellis, D. A. (1948). Surface areas of proteins. I. Surface areas and heats of absorption1. *Journal of the American Chemical Society*, *70*(11), 3563–3569.

Borges, A. C., Eyholzer, C., Duc, F., Bourban, P.-E., Tingaut, P., Zimmermann, T., et al. (2011). Nanofibrillated cellulose composite hydrogel for the replacement of the nucleus pulposus. *Acta Biomaterialia*, *7*(9), 3412–3421.

Brunauer, S., Emmett, P. H., & Teller, E. (1938). Adsorption of gases in multimolecular layers. *Journal of the American Chemical Society*, *60*(2), 309–319.

Cai, J., Kimura, S., Wada, M., Kuga, S., & Zhang, L. (2008). Cellulose aerogels from aqueous alkali hydroxide–urea solution. *ChemSusChem*, *2*(1–2), 149–154.

Cai, J., Liu, S., Kimura, S., Wada, M., Kuga, S., & Zhang, L. (2012). Cellulose–Silica nanocomposite aerogels by in Situ formation of silica in cellulose gel. *Angewandte Chemie International Edition*, *51*(9), 2076–2079.

Cai, H., Sharma, S., Liu, W., Mu, W., Liu, W., Zhang, X., et al. (2014). Aerogel microspheres from natural cellulose nanofibrils and their application as cell culture scaffold. *Biomacromolecules*, *15*(7), 2540–2547.

Capadona, J. R., Shanmuganathan, K., Tyler, D. J., Rowan, S. J., & Weder, C. (2008). Stimuli-responsive polymer nanocomposites inspired by the sea cucumber dermis. *Science*, *319*(5868), 1370–1374.

Chen, S., Schueneman, G., Pipes, R. B., Youngblood, J., & Moon, R. J. (2014). Effects of crystal orientation on cellulose Nanocrystals–cellulose acetate nanocomposite fibers prepared by dry spinning. *Biomacromolecules*, *15*(10), 3827–3835.

Chen, W., Li, Q., Wang, Y., Yi, X., Zeng, J., Yu, H., et al. (2014). Comparative study of aerogels obtained from differently prepared nanocellulose fibers. *ChemSusChem*, *7*(1), 154–161.

Cheow, W. S., Ng, M. L. L., Kho, K., & Hadinoto, K. (2011). Spray-freeze-drying production of thermally sensitive polymeric nanoparticle aggregates for inhaled drug delivery: Effect of freeze-drying adjuvants. *International Journal of Pharmaceutics*, *404*(1–2), 289–300.

Deville, S. (2008). Freeze-Casting of porous ceramics: A review of current achievements and issues. *Advanced Engineering Materials*, *10*(3), 155–169.

Ebert, H.-P. (2011). Thermal properties of aerogels. In M. A. Aegerter, N. Leventis, & M. M. Koebel (Eds.), *Aerogels handbook* (pp. 537–564). New York: Springer.

Fischer, F., Rigacci, A., Pirard, R., Berthon-Fabry, S., & Achard, P. (2006). Cellulose-based aerogels. *Polymer*, *47*(22), 7636–7645.

Fricke, J., & Emmerling, A. (1992). Aerogels—Preparation, properties, applications. In *Chemistry, spectroscopy and applications of sol-gel glasses*. pp. 37–87. Springer.

Fricke, J. (1986). Aerogels. *Springer proceedings in physics*,

Fricke, J. (1988). Aerogels—highly tenuous solids with fascinating properties. *Journal of Non-Crystalline Solids*, *100*(1–3), 169–173.

Ganster, J., Fink, H. P. (1999). Physical constants of cellulose. Polymer Handbook: E.H. Immergut, E.A. Grulke.

García-González, C. A., Alnaief, M., & Smirnova, I. (2011). Polysaccharide-based aerogels—Promising biodegradable carriers for drug delivery systems. *Carbohydrate Polymers*, *86*(4), 1425–1438.

Gavillon, R., & Budtova, T. (2008). Aerocellulose: New highly porous cellulose prepared from cellulose-NaOH aqueous solutions. *Biomacromolecules*, *9*(1), 269–277.

Gibson, L. J., & Ashby, M. E. (1999). *Cellular solids. Structure and properties*. Cambridge Solid Press.

Gronauer, M., Kadur, A., & Fricke, J. (1986). Mechanical and acoustic properties of silica aerogel. In P. D. J. Fricke (Ed.), *Aerogels* (pp. 167–173). Berlin, Heidelberg: Springer.

Gustafsson, S. E., Karawacki, E., & Khan, M. N. (1979). Transient hot-strip method for simultaneously measuring thermal conductivity and thermal diffusivity of solids and fluids. *Journal of Physics D: Applied Physics*, *12*(9), 1411.

Hüsing, N., & Schubert, U. (1998a). Aerogele-luftige Materialien: Chemie, Struktur und Eigenschaften. *Angewandte Chemie*, *110*(1–2), 22–47.

Hüsing, N., & Schubert, U. (1998b). Aerogels—Airy materials: Chemistry, structure, and properties. *Angewandte Chemie International Edition*, *37*(1–2), 22–45.

Hoepfner, S., Ratke, L., & Milow, B. (2008). Synthesis and characterisation of nanofibrillar cellulose aerogels. *Cellulose*, *15*(1), 121–129.

Huang, H.-J., Yuan, W.-K., & Chen, X. D. (2006). Microencapsulation based on emulsification for producing pharmaceutical products: A literature review. *Developments in Chemical Engineering and Mineral Processing*, *14*(3–4), 515–544.

Hult, E. L., Larsson, P. T., & Iversen, T. (2001). Cellulose fibril aggregation—an inherent property of kraft pulps. *Polymer*, *42*(8), 3309–3314.

Hunter, R. J. (2001). *Foundations of colloid science*. Oxford: University Press.

Innerlohinger, J., Weber, H. K., & Kraft, G. (2006). Aerocellulose: Aerogels and aerogel-like materials made from cellulose. *Macromolecular Symposia*, *244*(1), 126–135.

Jennings, T. A. (1999). *Lyophilization: Introduction and basic principles*. CRC Press.

Jones, S. M. (2006). Aerogel: Space exploration applications. *Journal of Sol-Gel Science and Technology*, *40*(2–3), 351–357.

Kaganer, M. G. (1969). Thermal Insulation in Cryogenic Engineering. Israel Program for Scientific Translations (1969) Jerusalem.

Kiani, H., & Sun, D.-W. (2011). Water crystallization and its importance to freezing of foods: A review. *Trends in Food Science & Technology*, *22*(8), 407–426.

Kistler, S. S. (1931). Coherent expanded aerogels and jellies. *Nature*, *127*(3211), 741.

Kistler, S. S. (1932). Coherent expanded-aerogels. *The Journal of Physical Chemistry*, *36*(1), 52–64.

Kistler, S. S. (1934). The relation between heat conductivity and structure in silica aerogel. *The Journal of Physical Chemistry*, *39*(1), 79–86.

Kobayashi, Y., Saito, T., & Isogai, A. (2014). Aerogels with 3D ordered nanofiber skeletons of liquid-crystalline nanocellulose derivatives as tough and transparent insulators. *Angewandte Chemie International Edition*, *53*(39), 10394–10397.

Koebel, M., Rigacci, A., & Achard, P. (2012). Aerogel-based thermal superinsulation: An overview. *Journal of Sol-Gel Science and Technology*, *63*(3), 315–339.

Koga, H., Saito, T., Kitaoka, T., Nogi, M., Suganuma, K., & Isogai, A. (2013). Transparent, conductive, and printable composites consisting of TEMPO-Oxidized nanocellulose and carbon nanotube. *Biomacromolecules*, *14*(4), 1160–1165.

Korhonen, J. T., Kettunen, M., Ras, R. H. A., & Ikkala, O. (2011). Hydrophobic nanocellulose aerogels as floating, sustainable, reusable, and recyclable oil absorbents. *ACS Applied Materials & Interfaces*, *3*(6), 1813–1816.

Liapis, A. I., Pim, M. L., & Bruttini, R. (1996). Research and development needs and opportunities in freeze drying. *Drying Technology*, *14*(6), 1265–1300.

Malecki, G. J., Shinde, P., Morgan, A. I., & Farkas, D. F. (1970). Atmospheric fluidized bed freeze drying. *Food Technology*, *24*, 601–603.

Mujumdar, A. S. (2014). *Handbook of industrial drying* (4th ed.). CRC Press.

Nguyen, S. T., Feng, J., Ng, S. K., Wong, J. P. W., Tan, V. B. C., & Duong, H. M. (2014). Advanced thermal insulation and absorption properties of recycled cellulose aerogels. *Colloids and Surfaces A: Physicochemical and Engineering Aspects*, *445*, 128–134.

Pääkkö, M., Vapaavuori, J., Silvennoinen, R., Kosonen, H., Ankerfors, M., Lindström, T., et al. (2008). Long and entangled native cellulose I nanofibers allow flexible aerogels and hierarchically porous templates for functionalities. *Soft Matter*, *4*(12), 2492–2499.

Pekala, R. W., Alviso, C. T., & LeMay, J. D. (1990). Organic aerogels: Microstructural dependence of mechanical properties in compression. *Journal of Non-Crystalline Solids*, *125*(1), 67–75.

Pierre, A. C., & Pajonk, G. M. (2002). Chemistry of aerogels and their applications. *Chemical Reviews*, *102*(11), 4243–4266.

Platzer, W., Wittwer, V., & Mielke, M. (1986). Solar transmission of aerogel pellets. In P. D. J. Fricke (Ed.), *Aerogels* (pp. 127–132). Berlin Heidelberg: Springer.

Reichenauer, G. (2000). Aerogels. In *Kirk-Othmer encyclopedia of chemical technology*. John Wiley & Sons, Inc.

Rouquerol, J., Avnir, D., Fairbridge, C. W., Everett, D. H., Haynes, J. H., & Pernicone, N. (1994). Recommendations for the characterization of porous solids. *Pure and Applied Chemistry*, *10*(66), 1739–1758.

Rudaz, C., Courson, R., Bonnet, L., Calas-Etienne, S., Sallée, H., & Budtova, T. (2014). Aeropectin: Fully biomass-based mechanically strong and thermal superinsulating aerogel. *Biomacromolecules*, *15*(6), 2188–2195.

Saito, T., Nishiyama, Y., Putaux, J.-L., Vignon, M., & Isogai, A. (2006). Homogeneous suspensions of individualized microfibrils from TEMPO-catalyzed oxidation of native cellulose. *Biomacromolecules*, *7*(6), 1687–1691.

Sehaqui, H., Salajková, M., Zhou, Q., & Berglund, L. A. (2010). Mechanical performance tailoring of tough ultra-high porosity foams prepared from cellulose I nanofiber suspensions. *Soft Matter*, *6*(8), 1824–1832.

Sehaqui, H., Zhou, Q., & Berglund, L. A. (2011). High-porosity aerogels of high specific surface area prepared from nanofibrillated cellulose (NFC). *Composites Science and Technology*, *71*(13), 1593–1599.

Sehaqui, H., Zhou, Q., Ikkala, O., & Berglund, L. A. (2011). Strong and tough cellulose nanopaper with high specific surface area and porosity. *Biomacromolecules*, *12*(10), 3638–3644.

Sescousse, R., Gavillon, R., & Budtova, T. (2011). Aerocellulose from cellulose–ionic liquid solutions: Preparation, properties and comparison with cellulose–NaOH and cellulose–NMMO routes. *Carbohydrate Polymers*, *83*(4), 1766–1774.

Shanmugam, S. (2015). Granulation techniques and technologies: Recent progresses. *BioImpacts: BI*, *5*(1), 55–63.

Shi, J., Lu, L., Guo, W., Sun, Y., & Cao, Y. (2013). An environment-friendly thermal insulation material from cellulose and plasma modification. *Journal of Applied Polymer Science*, *130*(5), 3652–3658.

Silva, T. C. F., Habibi, Y., Colodette, J. L., Elder, T., & Lucia, L. A. (2012). A fundamental investigation of the microarchitecture and mechanical properties of tempo-oxidized nanofibrillated cellulose (NFC)-based aerogels. *Cellulose*, *19*(6), 1945–1956.

Svagan, A. J., Samir, M. A., Berglund, L. A., et al. (2008). Biomimetic foams of high mechanical performance based on nanostructured cell walls reinforced by native cellulose nanofibrils. *Advanced Materials-Deerfield Beach Then Weinheim*, *20*(7), 1263–1269.

Tamon, H., Ishizaka, H., Yamamoto, T., & Suzuki, T. (2000). Influence of freeze-drying conditions on the mesoporosity of organic gels as carbon precursors. *Carbon*, *38*(7), 1099–1105.

Tan, C., Fung, B. M., Newman, J. K., & Vu, C. (2001). Organic aerogels with very high impact strength. *Advanced Materials*, *13*(9), 644–646.

Thybo, P., Hovgaard, L., Andersen, S. K., & Lindeløv, J. S. (2008). Droplet size measurements for spray dryer scale-up. *Pharmaceutical Development and Technology*, *13*(2), 93–104.

Werly, E. F., & Baumann, E. K. (1964). Production of submicronic powder by spray-freezing. *Archives of Environmental Health: An International Journal*, *9*(5), 567–571.

Wong, J. C. H., Kaymak, H., Brunner, S., & Koebel, M. M. (2014). Mechanical properties of monolithic silica aerogels made from polyethoxydisiloxanes. *Microporous and Mesoporous Materials*, *183*, 23–29.